JOURNAL OF GEOPHYSICAL RESEARCH, VOL. 114, A04201, doi:10.1029/2008JA013712, 2009

Geomagnetic signatures of auroral substorms preceded by pseudobreakups

A. Kullen,[1] S. Ohtani,[2] and T. Karlsson[3]

Received 29 August 2008; revised 19 January 2009; accepted 27 January 2009; published 3 April 2009.

[1] The evolution of ten growth-phase pseudobreakups and subsequent substorms, identified in Northern Hemisphere Polar UV images during winter 1998–1999, are compared to the *AE* index, the unified *PC* indices, and GOES *B* field data. Comparing substorm onset (auroral breakup) with GOES data and *AE* and *PC* indices, it is found that an exact onset determination from these parameters is in most cases not possible. The three weakest substorms leave no clear signatures in the auxiliary parameters. For the other events, the *AE* increase appears with a time delay of 5–15 min after onset. The *PC* indices increase, as expected, before the *AE* index. The time span between *PC* increase and onset varies widely (−26 to 5 min). A tail dipolarization is seen in GOES data with a time delay of 2–31 min after onset. The dipolarization delay at geosynchronous orbit appears because of the GOES displacement from the tail onset region. Using the mapped GOES distance from the auroral breakup region as an estimate of GOES displacement from the breakup source region, we find that the tail dipolarization region expands in average with an azimuthal speed of 0.22 MLT min^{-1} and an equatorward speed of 0.09° min^{-1}. Pseudobreakups leave hardly any signature in *AE* or *PC* index data except in the four strongest substorm cases. In these cases, a bump appears in the *PC* indices during the pseudobreakup. A bump in geosynchronous *B* field data is found only in those two cases where GOES is located very close to the pseudobreakup tail source region.

Citation: Kullen, A., S. Ohtani, and T. Karlsson (2009), Geomagnetic signatures of auroral substorms preceded by pseudobreakups, *J. Geophys. Res.*, *114*, A04201, doi:10.1029/2008JA013712.

1. Introduction

[2] One of the most important manifestations of energy coupling between the solar wind and the magnetosphere are magnetospheric substorms. The start of an auroral substorm is preceded by a growth-phase during which the entire auroral oval expands toward lower latitudes [*McPherron*, 1972]. Substorm onset starts at the most equatorward discrete arc at a fixed distance of 3–4 degrees from the equatorward boundary of the UV oval [*Gerard et al.*, 2004]. The developing auroral surge expands in poleward and westward direction. Some authors claim that the westward traveling surge in fact consists of subsequent onset intensifications that are more and more duskwardly displaced [e.g., *Rostoker et al.*, 1980]. Substorm expansion is dominated by dynamic displays of bright, discrete auroral arcs. The most commonly observed auroral forms during expansion and recovery include multiple auroral intensifications within the oval, intensifications along the poleward oval boundary (PBIs) [*Lyons et al.*, 1999], and auroral streamers [*Henderson et al.*, 1998].

[1]Swedish Institute of Space Physics, Uppsala, Sweden.
[2]Johns Hopkins University Applied Physics Laboratory, Laurel, Maryland, USA.
[3]Division of Space and Plasma Physics, School of Electrical Engineering, KTH, Stockholm, Sweden.

0148-0227/09/2008JA013712$09.00

[3] The auroral signatures of a substorm are accompanied by large-scale changes in the magnetotail topology. During the growth phase, the magnetotail magnetic field (*B* field) becomes more stretched [*Kokubun and McPherron*, 1981], whereas the expansion phase is characterized by the dipolarization of the tail *B* field [*Cummings et al.*, 1968]. During substorm recovery the tail returns to its ground state with a moderately stretched tail *B* field. The increase of open magnetic flux during the growth phase results in a larger polar cap. The enhanced plasma convection during active geomagnetic times causes an earthward motion of the inner plasma sheet boundary, which is manifested in a more equatorward location of the low-latitude auroral oval boundary [*Lyons et al.*, 1999].

[4] The *B* field stretching is associated with an intensification and thinning of the tail current sheet, while the magnetic field dipolarization is connected to a disruption of the tail current. There is no generally accepted model that accounts for all observed features around substorm onset, but it has been agreed on that the initial auroral breakup is connected to the disruption of the tail current that starts near the inner edge of the plasma sheet at 6–10 R_E from the Earth [*Lui*, 1991; *Kennel*, 1992]. The disrupted tail current closes via the westward electrojet through the ionosphere. The formation of a near-Earth neutral line (NENL) is observed further downtail at about 15–25 R_E, and is connected to the observed *B* field dipolarization and strong earthward plasma flows. According to *Baker et al.* [2002],

the current disruption in the inner tail appears as a consequence of the strong earthward plasma flows that is decelerated in the high-pressure plasma region in the near-Earth tail. Others claim that it is the other way around, a NENL forms as a consequence of rarefaction waves propagating tailward from the current sheet disruption region [e.g., *Lui*, 1996]. Observations that the *B* field dipolarization starts locally [*Ohtani et al.*, 1991] and spreads azimuthally [*Nagai*, 1982; *Liou et al.*, 2002], and radially outward [*Jacquey et al.*, 1991; *Ohtani et al.*, 1992] as well as inward [*Ohtani*, 1998], has been interpreted in favor for the tail current disruption model. A further observation in favor of that model is that midtail fast flows are rarely followed by dipolarization at geosynchronous orbit [*Ohtani et al.*, 2006].

[5] Substorms are known to develop predominantly during a southward direction of the interplanetary magnetic field (IMF). However, they may occur even during northward IMF [*Hsu and McPherron*, 2003]. In a large statistical study *Kullen and Karlsson* [2004] found that 28% of all substorms identified on Polar UV images appear during extended periods of (in most cases weakly) northward IMF. These substorms are typically weak and short-lived and appear on a contracted oval, as can be expected from the strong correlation between IMF B_Z and substorm intensity. The auroral electrojet (*AE*) index, which describes the maximum amount of auroral activity within the auroral zone, has highest values for southward IMF in connection with high IMF magnitude and solar wind velocity [*Akasofu*, 1980].

[6] *Kullen and Karlsson* [2004] showed that at least 14% of all substorm onsets are preceded by auroral activation that is not followed by a global expansion. These so-called pseudobreakups have been known for a long time [*Elvey*, 1957; *Akasofu*, 1964]. Growth-phase pseudobreakups take place a few to some tens of minutes before the main substorm breakup [*Koskinen et al.*, 1993], are short-lived (5–16 min) and are localized (although, occasionally they may have a longitudinal extension of several hours magnetic local time (MLT) [*Aikio et al.*, 1999]). Although most studies focus on growth-phase pseudobreakups, the majority of pseudobreakups appears during quiet times (58%) or during the late substorm recovery phase (25%) [*Kullen and Karlsson*, 2004, and references therein]. Each type of pseudobreakup appears during a characteristic set of solar wind conditions: isolated pseudobreakups (called "single pseudobreakups" by *Kullen and Karlsson* [2004]) appear mainly during weakly northward IMF. Most growth-phase pseudobreakups appear after a 1–2 h long period of weakly southward IMF, just before a rather small or expanding substorm develops. Recovery-phase pseudobreakups develop at the end of a highly active substorm recovery. A dynamic recovery is commonly observed after an IMF turn from negative to positive IMF B_Z. A recovery-phase pseudobreakup appears typically as a single brightening near the poleward oval boundary while typically, the middle parts of the oval already start to erode. Long periods of strongly southward IMF with recurrent substorms are devoid of pseudobreakups. Common for all pseudobreakups is their appearance during low solar wind velocity, IMF magnitude and a near zero IMF B_Z. This means that their occurrence is most probable when the magnetic energy flux of the solar wind is low [*Kullen and Karlsson*, 2004].

[7] Many authors claim, there is a continuum of states between pseudobreakups as the smallest possible type of substorm and large substorms [e.g., *Aikio et al.*, 1999; *Nakamura et al.*, 1994]. Observational results support this view: 1. The average solar wind conditions change smoothly from very small to very large values of the solar wind magnetic energy flux between pseudobreakups, and substorms of increasing strength [*Kullen and Karlsson*, 2004]. 2. Pseudobreakups have been found to be associated with the same ionospheric and magnetotail signatures as substorm breakups, the only difference being the global consequence. Magnetic field line dipolarization, energetic particle injections and fast ion flows in the tail can often be as intense as those of substorm onsets, but are short-lived and appear only locally [e.g., *Koskinen et al.*, 1993; *Ohtani et al.*, 1993]. Note that even PBIs have similar characteristics as pseudobreakups, the only difference is their (multiple) appearance within the course of a substorm [*Lyons et al.*, 1999], which makes a clear distinction between pseudobreakups and PBIs difficult.

[8] As substorm breakup starts close to the inner plasma sheet boundary, while most (even growth-phase) pseudobreakups seem to have a more tailward source region [*Sergeev et al.*, 1996, and references therein]. *Rostoker* [2002] suggested that auroral intensifications originating in the far tail may involve a different formation mechanism than those occurring near the equatorward oval boundary. In contrast to *Rostoker* [2002], *Sergeev et al.* [1996] suggest that all small auroral intensifications (pseudobreakups, substorm breakup and PBIs) are basically the same type of minimum energy release events in the magnetosphere. The reason that only those auroral activations expand globally, that have their source region very close to the Earth, is according to *Sergeev et al.* [1996] that the intensity of the dissipation process is largest in the near-Earth tail. Such a scenario, however, explains neither the more tailward source region of substorms that occur on a contracted oval during quiet times [*Lui et al.*, 1976; *Kullen and Karlsson*, 2004] nor growth-phase pseudobreakups located equatorward of the following substorm breakup [*Nakamura et al.*, 1994].

[9] While isolated pseudobreakups can be interpreted as very small substorms (they often have a larger longitudinal extension and a longer lifetime than growth-phase pseudobreakups), and recovery pseudobreakups may be regarded as a special type of PBI due to their location close to the poleward oval boundary, the cause of growth-phase pseudobreakups remains unclear. The question what prevents growth-phase pseudobreakups from expanding into a global substorm has been asked by many authors. Most authors assume the rate of the solar wind–energy transfer into the magnetosphere is ultimately responsible for whether a growth-phase pseudobreakup occurs or not. However, depending on solar wind conditions of the studied event, each author draws a different conclusion: *Koskinen et al.* [1993] and *Nakamura et al.* [1994] proposed that growth-phase pseudobreakups occur before enough energy is stored in the tail. *Pulkkinen et al.* [1998] and *Rostoker* [1998] speculated that a continuously increasing energy input from the solar wind suppresses the development of a full substorm, while *Partamies et al.* [2003] suggested that a

sudden energy decrease just before an auroral intensification may prevent a global expansion.

[10] The goal of this work is to obtain a better understanding of why some substorms are preceded by growth-phase pseudobreakups while others are not. The main focus is on possible deviations between substorms that appear after growth-phase pseudobreakups from "normal" substorms that are not accompanied by growth-phase pseudobreakups. To investigate this, 10 growth-phase pseudobreakups and subsequent substorms are examined in detail. The auroral evolution is compared to B field variations in the solar wind, high-latitude ionosphere, and in the near-Earth magnetosphere. The observations are compared to results from previous substorm and pseudobreakup studies.

2. Instrumentation

[11] The UV camera on board the Polar satellite produces global images of the auroral oval every 37 s in the far ultraviolet region of the spectrum using four narrow band filters with integration times of 18 and 36 s, respectively [*Torr et al.*, 1995]. For the onset determination all existing UV images are used, to get an as high time resolution as possible. For a detailed investigation of the auroral substorm, only LBH long (160–180 nm) images with the long integration time of 36 s are taken. In this wavelength range emissions are not significantly absorbed in the atmosphere, thus the emission intensity is approximately proportional to the electron energy flux into the ionosphere [*Germany et al.*, 1998]. The resolution of the UV imager is about 0.5° in latitude at apogee: thus a single pixel projected to 100 km altitude from apogee is approximately 50 × 50 km. Away from apogee the imager can detect even smaller spatial scales. Because of a spacecraft wobble in one spacecraft direction, the effective pixel size sometimes increases up to 50 × 250 km. Any spatial determination of the onset region is correct within the given resolution only.

[12] For an examination of the solar wind conditions 1-min averaged OMNI (Operating Missions as Nodes on the Internet) data are used. They are provided on the OMNIWeb (http://omniweb.gsfc.nasa.gov). The data set consists of solar wind measurements from that solar wind monitor which is closest to the dayside magnetopause. The data are already propagated in time to the Earth's bow shock. A detailed documentation is given by *King and Papitashvili* [2005].

[13] The AE index is derived from geomagnetic variations in the horizontal component, observed from up to 12 stations that are located within a fixed latitudinal band, covering the auroral zone. It is defined as the difference between the value from the station with the largest (AU) and the station with the smallest geomagnetic variations (AL) at each given point in time. The AE index represents the overall activity of the westward and eastward auroral electrojets. Thus, it is a good estimate of how the auroral substorm develops on a global scale, as long as the oval lies within the given latitudinal band. As the final AE index values are not yet available for the time period covered by this study, AE quick-look plots are used (available at http:/swdcdb.kugi.kyoto-u.ac.jp/aedir/ae1/quick.html). The quick-look plots for winter 1998–1999 are derived from 8 out of the 12 AE stations, using unchecked data. Of the events studied here, the data was derived from all 8 stations, except for one event (6 December 1998) where the index was derived from 7 stations.

[14] The polar cap (PC) index, introduced by *Troshichev et al.* [1979, 1988], monitors geomagnetic activity over the northern and southern polar caps. As the B field variation over the polar cap has been shown to be a good estimate of the merging electric field E_m in the solar wind [*Kan and Lee*, 1979] the PC index is often used as a proxy for the amount of energy transferred from the solar wind and IMF to the magnetosphere through direct driving. The northern and southern PC indices are continuously derived from geomagnetic data obtained at Qaanaaq/Thule (Greenland) and Vostok (Antarctica), respectively. In the present study, an improved version of the northern and southern PC indices is used. These have been provided directly from the Danish Meteorological Institute (P. Stauning, personal communication, 2008), as an online version is not yet available. For the new, unified PC indices, the calculation procedures of the northern and southern indices have been unified, and a larger data set is used for the derivation of the coefficients [*Troshichev et al.*, 2006]. The main difference between the unified procedure and the earlier calculations is the subtraction of a quiet level before index values are calculated from the magnetic recordings. Deviations in the northern and southern PC index [*Lukianova et al.*, 2002] that have been caused by different calculation procedures are eliminated in the new version. *Troshichev et al.* [2006] showed that statistically, the unified PC indices are linearly proportional to the merging electric field $E_m = vB_T\sin^2(\Theta/2)$, where v is the solar wind velocity, B_T is the transverse IMF component, and Θ is the IMF clock angle. Thus, the PC indices have the same units as the merging electric field E_m: (mV/m).

[15] For an examination of geosynchronous magnetic signatures, 1-min averaged magnetometer data from the GOES 8 and GOES 10 satellites are used. The GOES satellites are located approximately in the equatorial plane at a geocentric distance of 6.62 R_E. The measurements are given in the VDH coordinate system. In this coordinate system, H is antiparallel to the dipole axis and is positive northward, V points radially outward and is parallel to the magnetic equator, D completes a right-hand orthogonal system and is positive eastward. The magnetic field stretching (dipolarization) during substorm growth phase (expansion) can be easily studied by examining the H component.

3. Event Selection

[16] The events used in this work are taken from the statistical study of pseudobreakups and substorms by *Kullen and Karlsson* [2004]. In that study, all substorm-like activity that appears in the global auroral images of the Polar UV imager in the Northern Hemisphere during three winter months in 1998–1999 has been selected (except auroral brightenings on the dayside part of the oval). In a second step, all events have been classified as either substorms or pseudobreakups. The classification was based solely on the analysis of the auroral evolution after breakup, as it appears on the Polar UV images. Because of the limited resolution of the images, it is not possible to discern single discrete

Table 1. Time Delay Between Auroral Substorm Breakup, *AE* Index Increase, and *PC* Index Increase

	Substorm Onset		Time Delay After Substorm Onset (min)		
Case	Date	Time (UT)	*AE* Increase	*PCN* Increase	*PCS* Increase
1	7 Jan 1999a	0328	-	-	-
2	7 Jan 1999b	0642	-	-	-
3	28 Dec 1998	1119	+10	-	-
4	6 Dec 1998	0447	+10	-	-
5	14 Dec 1998	0852	+15	−3	-
6	23 Dec 1998	0613	+5	+4	-
7	3 Dec 1998	0707	+11	−25	−26
8	25 Feb 1999	0354	+6	+3	−8
9	24 Feb 1999	1029	+11	−16	+5
10	15 Jan 1999	0816	+15	−17	−12

arcs, i.e., the poleward motion of the onset arc cannot be used as a criterion for which type of auroral activation takes place. Instead, the dawn-duskward expansion of the breakup region is used as indicator for whether a pseudobreakup or a substorm appears. Those auroral breakups that do not show a considerable azimuthal expansion of the original breakup region have been classified as pseudobreakups, all other events as substorms. In a next step, all pseudobreakup events have been subdivided into growth-phase pseudobreakups, recovery pseudobreakups and isolated pseudobreakups. Those pseudobreakups that appear close to (<30 min before) substorm onset, have been classified as growth-phase pseudobreakups (57 events). For more details about selection criteria and event classification we refer to *Kullen and Karlsson* [2004].

[17] In the present study, we focus on those 10 growth-phase pseudobreakups and subsequent substorms for which geosynchronous B field data is available near midnight, i.e., one of the GOES satellites is located in the magnetotail between 3 MLT and 21 MLT during the growth-phase pseudobreakup. Dates and onset times of all 10 substorms are listed in Table 1. The events are numbered from 1 to 10 after increasing substorm strength (maximum *AE* value). From here on we refer to each event according to the case number, given in Table 1. Also shown in Table 1 are the time delays between substorm onset, *AE* increase, northern *PC* increase (*PCN*) and southern *PC* increase (*PCS*). These are discussed further down. In the work of *Kullen and Karlsson* [2004] the onset times have been roughly estimated from UV images sheets with a time span of 4–6 min between each image. To get more exact breakup times, they are redetermined by using every existing Polar UV image. This improves the onset-time determination considerably: In five events, the UV image time resolution is about 40 s (cases 3, 4, 6, 8 and 10), in 3 events about 60 s (cases 1, 2, and 5), and in the remaining two events about 1.5 min (case 9) and 2 min (case 7), respectively. Substorm (and pseudobreakup) start is defined here as the point in time where the auroral intensification for the first time becomes clearly visible in the Polar UV images. Note, the development between a first, often extremely weak brightening, and a clearly identified onset can take up to a few minutes for small substorms. Thus, for such a substorm the visually determined auroral breakup times may be up to a few minutes later than the actual auroral breakup.

4. Results

4.1. Magnetic Field Signatures During Pseudobreakups and Subsequent Substorms

[18] In Figure 1, the magnetic field variations in the solar wind, in the polar cap, in the auroral zone, and in the near-Earth tail are shown during a 5 h time frame around each of the studied growth-phase pseudobreakups and subsequent substorms. All data are given with 1-min resolution. As in Table 1, the plots are sorted according to the maximum *AE* value with the weakest event on the top left corner (case 1), and the strongest event in the bottom right corner (case 10). The blue and green shaded vertical bars mark growth-phase pseudobreakups and substorms, respectively. Substorm activity (mainly substorm recoveries and isolated pseudobreakups) taking place before the growth-phase pseudobreakup is not shown here. In the first panel, IMF B_Z (black) and solar wind merging electric field E_m (red) from the OMNI data set are shown. The OMNI data are already time-shifted to correspond the time, when the solar wind has reached the Earth bow shock. The second panel contains the northern (black) and southern (red) unified *PC* indices. The *AE* index is plotted in the third panel. The fourth panel shows the magnetic field variations of B_H at geosynchronous orbit. As the B_H component is near the equatorial plane approximately in northward direction, increasing B_H corresponds to B field dipolarization, decreasing B_H corresponds to B field stretching. The average quiet time magnetic field (K_P = 0) of the T89 magnetosphere model [*Tsyganenko*, 1989] is subtracted from the GOES B field data to make the local B field variations more visible.

4.1.1. Solar Wind Merging Magnetic Field and IMF B_Z

[19] From *Kullen and Karlsson* [2004] it is known that growth-phase pseudobreakups appear typically after a 1–2 h long period of weakly southward IMF. Often an IMF northward turning appears just before or during the subsequent substorm. In the limited subset, analyzed in the present study, these IMF conditions are not seen very clearly. In the *Kullen and Karlsson* [2004] study, 5 min averaged solar wind data from the ACE satellite was used. The improved propagation time calculation and better time resolution of OMNI solar wind data, as well as a more correct onset time determination of the present study, reveal that most growth-phase pseudobreakups appear during or up to 5 min after IMF B_Z is (temporarily) near zero due to a B_Z sign change or short-time B_Z decrease to very small values. The E_m curves deviate strongly from case to case. During the hour before the growth-phase pseudobreakup appears, E_m is slightly enhanced in half of the cases. However, no clear connection with pseudobreakup or substorm onset is found.

4.1.2. *AE* Index

[20] In statistical studies, often a sharp rise in the *AE* index is used as an approximation for substorm onset (e.g., *Janzhura et al.* [2007] defining onset as local maximum of first derivative of a smoothed *AE* curve). With the more correct onset determination in the present study, where substorm onset is defined as the start of the auroral breakup

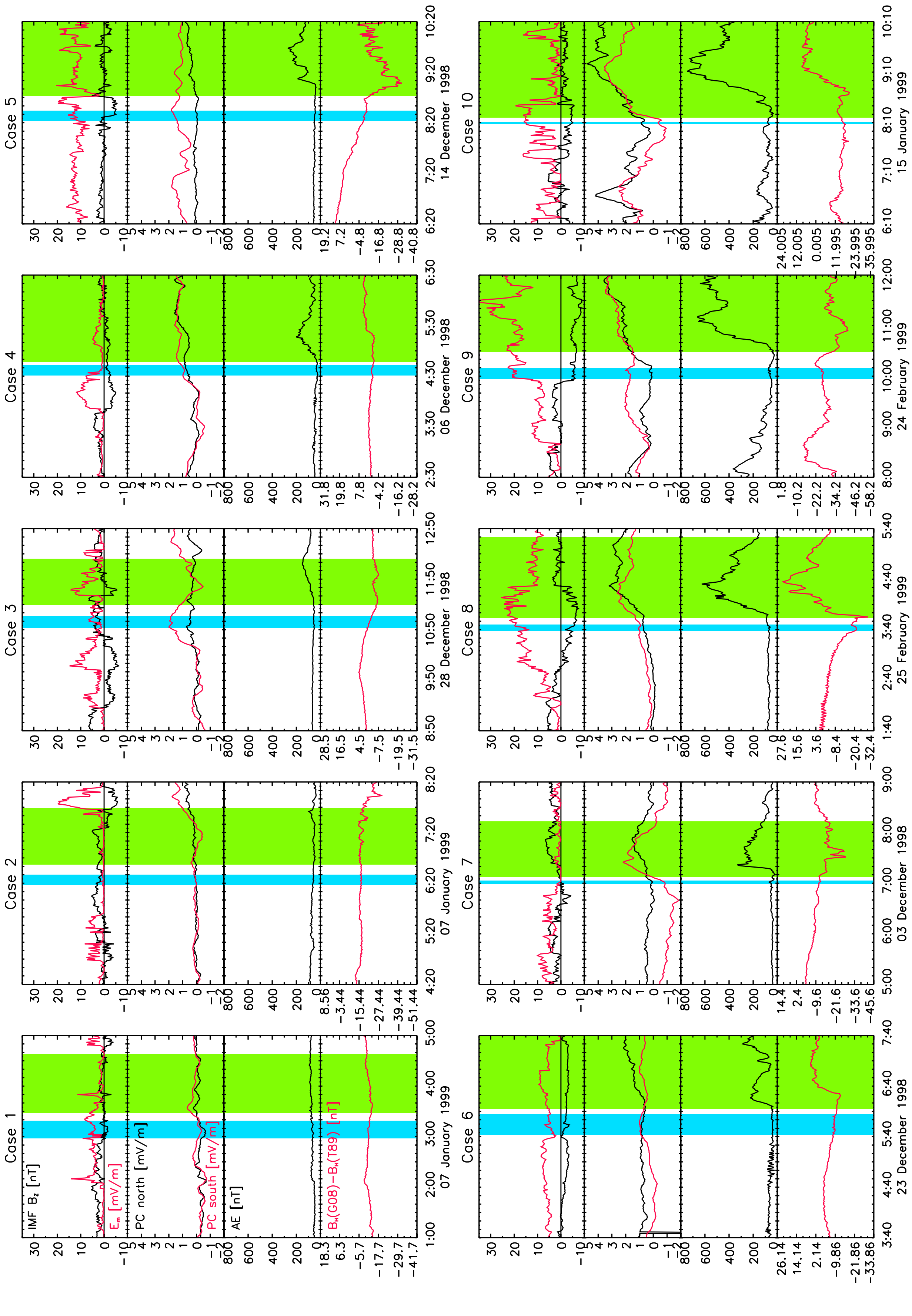
Case 1
07 January 1999
Case 2
07 January 1999
Case 3
28 December 1998
Case 4
06 December 1998
Case 5
14 December 1998
Case 6
23 December 1998
Case 7
03 December 1998
Case 8
25 February 1999
Case 9
24 February 1999
Case 10
15 January 1999
IMF B_z [nT]
E_m [mV/m]
PC north [mV/m]
PC south [mV/m]
AE [nT]
B_x(G08)−B_x(T89) [nT]

Figure 1

[e.g., *Liou et al.*, 1999, and references therein], it is possible to investigate how well the start of the *AE* increase corresponds to the real onset of the auroral substorm.

[21] Comparing substorm onset (left boundary of the green shaded area in Figure 1) with the start of a sharp *AE* increase, it is found that nearly all substorm breakups are connected to such an increase, however in most cases a sharp increase of the *AE* curve starts with a considerable time delay. The two weakest substorms (cases 1 and 2), and the pseudobreakups leave no significant signature in the *AE* index. The reason may be the relatively weak brightness of the breakup region, its small east-west extension, and/or a strong contraction of the oval, so that most *AE* stations are situated equatorward of the oval. As shown below, the equatorward oval boundary is indeed on very high latitudes during the two weakest substorms and during nearly all pseudobreakups. This is typical for the near zero IMF B_Z values during which these events occur [*Gerard et al.*, 2004].

[22] The time span between auroral breakup and the start of a strong *AE* increase, as well as possible northern and southern *PC* index increases are given explicitly in Table 1. Numbers are given only for those events where an obvious connection between index increase and substorm is found. As mentioned above, substorm onset may possibly have started a few minutes earlier then the visually determined onset times, while it can be excluded that substorm onset starts after the visually determined onset time. Thus, the numbers given in Table 1, column 3 are minimum values for the time delays between substorm onset and sharp *AE* increase. It is found that in our data set, a sharp *AE* increase starts at least 5–15 min after substorm onset.

4.1.3. *PC* Index

[23] The (unified) *PC* index has been shown by *Troshichev et al.* [2006] to be linearly proportional to the solar wind merging *E* field. However, the correlation with E_m is good only during southward IMF, where, because of the open field line configuration of the polar cap, the solar wind *E* field maps directly to ionospheric heights [*Troshichev et al.*, 2006]. This is probably the reason why no clear connection between *PC* index and merging *E* field is found in our data set. IMF B_Z is weakly southward or even northward during most substorms. The best (however still not good) correlation between E_m and *PC* index is found for case 8 and case 9 with strongly southward IMF during substorm expansion. We conclude that the *PC* indices cannot be regarded as solar wind energy transfer indicators for our data set.

[24] The (unified) *PC* index is known to correlate well also with the *AE* index [*Janzhura et al.*, 2007]. A rise in the *PC* index curve is expected to appear 3–10 min before a sharp *AE* increase [*Troshichev and Lukianova*, 2002]. In our data set, a connection between the *PC* index curve and the *AE* index curve is seen only in the stronger substorm events. In the four weakest substorm cases no clear correlation is found (cases 1–4). The northern *PC* index has a stronger resemblance with the *AE* index curve than the southern *PC* index, except for case 7. As expected from *Janzhura et al.* [2007], both *PC* indices rise before the *AE* index. The time span between substorm onset (auroral breakup) and start of the *PC* index increase is given in Table 1 for those events where a clear connection between *PC* index increase and substorm onset could be found. This time span varies strongly, even for the northern *PC* index: in the four weakest events (cases 1–4), it is not possible to associate northern *PC* index increases with substorm onsets, in three events (cases 5, 6, and 8), the northern *PC* increase starts very close to substorm onset, in the remaining events (cases 7, 9 and 10), the northern *PC* increases 16–25 min before onset. Thus, despite the large time delays between *AE* and substorm onset in the present data set, the *AE* index is still a better substorm indicator than the *PC* indices.

[25] It is possible that pseudobreakups have an influence on the *PC* index curve. During the pseudobreakups preceding the four strongest substorms (cases 7–10), a bump in the southern *PC* index curve can be discerned, which is clearly pronounced in the two strongest substorm events. In these two events, a similar bump appears even in the northern *PC* index curve. In three of the four events with southern *PC* index bumps, an internal magnetospheric source is much more probable than an external solar wind driver: no signature is found in E_m, IMF B_Z, or the solar wind pressure (not shown). Solar wind pressure jumps are the most probable candidate for causing auroral intensifications [e.g., *Zhou and Tsurutani*, 1999] and may even trigger substorms [*Hsu and McPherron*, 2003]. Only in case 9, with strongly southward IMF, the bump could possibly be influenced by the local E_m maximum, and/or a solar wind pressure jump. Interestingly, the *PC* index signatures during the pseudobreakups, are in three of these four events (cases 8–10) more clearly pronounced than in the *AE* index showing no or only extremely weak signatures during pseudobreakups.

4.1.4. GOES Magnetic Field Data

[26] Studying the *B* field variation at geosynchronous orbit shows, the large dipolarization (B_H increase), which is expected to occur in connection with substorm onset [*Cummings et al.*, 1968], is found to appear in most cases with a large time delay. There are three exceptions: For the two weakest substorms (cases 1 and 2), no dipolarization is seen at all. In case 8, a *B* field dipolarization is registered only minutes after the auroral breakup. As shown below, this is the only event where GOES is located very close to the tail onset region. Several growth-phase pseudobreakups are connected to a small bump in B_H during (cases 4, 5 and 8) or just after the pseudobreakup (case 9). In only two events (cases 8 and 9), this bump is very clear. During the time interval between pseudobreakup and substorm breakup, growth-phase stretching continues in all cases,

Figure 1. Magnetic field variations in the solar wind, over the polar cap, in the auroral zone, and at geosynchronous orbit in the magnetotail for a 5 h interval around the growth-phase pseudobreakup (blue vertical bar) and subsequent substorm (green shaded region) for all 10 events. Shown for each case are IMF B_Z (in GSM coordinates) and the solar wind merging *E* field using OMNI solar wind data (first panel), the northern and southern unified *PC* indices (second panel), the *AE* index (third panel), and the B_H component (in VHS coordinates) of the tail *B* field at geosynchronous orbit from the GOES 8 and GOES 10 satellites, with the quiet time magnetosphere field from the T89 model subtracted (fourth panel).

except in case 10. The *B* field stretching continues in most cases at GOES location even after onset. For three events (cases 7, 9 and 10), a first, very weak dipolarization can be discerned in connection with substorm onset, while the large dipolarization appears much later.

4.2. Mapped GOES Location in the Auroral Ionosphere

[27] A time delay between substorm onset and the start of the tail dipolarization at geosynchronous orbit can be expected for those cases where GOES is displaced from the original tail onset location, as the tail dipolarization is known to start locally and spreads from there in all directions. Both azimuthal [*Nagai*, 1982; *Liou et al.*, 2002], and radial expansion of the tail dipolarization region [*Ohtani et al.*, 1992; *Ohtani*, 1998] are well documented. To be able to estimate the propagation speed of the tail dipolarization, we map GOES position to ionospheric heights. The distance between the mapped GOES position in the ionosphere and the auroral breakup is assumed to be the mapped distance between tail source region and GOES tail location. In a first step, the GOES position is mapped to the Polar UV images using the T96 magnetosphere *B* field model [*Tsyganenko*, 1995]. As input into the T96 model, hourly averaged solar wind data from ACE during the hour closest to the growth-phase pseudobreakup are taken. The model input data consist of IMF B_Y, IMF B_Z, solar wind ram pressure, and *Dst* index data. In a second step, the mapped GOES position is marked on each Polar UV image.

[28] The resulting plots with the mapped GOES position overlaid on Polar UV images show five different situations: (1) GOES maps into the auroral breakup region, (2) GOES appears equatorward of the oval, (3) GOES appears inside the oval but is strongly dawnwardly or duskwardly displaced from the auroral breakup, (4) GOES maps equatorward of the oval at substorm onset, later on, GOES appears inside the oval owing to an equatorward motion of the low-latitude oval boundary during substorm expansion, and (5) GOES maps to the poleward oval boundary.

[29] In Figure 2, cases 8, 2, 6 and 7 are shown as examples of the first four scenarios. Each row shows the temporal evolution of one growth phase pseudobreakup and the expansion of the subsequent substorm. In all cases the pseudobreakup appears in the second UV image (in case 6 it is seen also in the third image). Substorm onset appears in the fourth UV image (in case 6 in the fifth image) of each row. The plots give a polar view over the high-latitude Northern Hemisphere, with MLT-CGLat (Corrected Geomagnetic Latitude) coordinates overlaid on the Polar UV images in the LBHL mode. The color scale extends from 3.5 photons cm^{-2} s^{-1} to a maximum value that differs from case to case (row). For each case, the brightest pixel in the corresponding row defines the maximum value of the color scale. The mapped position of the GOES satellite is marked with a black cross in each plot. The plots in the first row of Figure 2 show the event (case 8) where GOES maps exactly to the pseudobreakup and very close to the following substorm breakup region, which suggests that GOES is located at (or at least very close to) the breakup source region in the magnetotail. This is the only event with an overlap between the mapped GOES position and pseudobreakup. In the second row is shown the only event (case 2) where GOES is situated equatorward of a rather contracted oval during the entire pseudobreakup and substorm evolution. The longitudinal substorm expansion is limited, and the oval does not widen considerably during the course of the substorm. We thus assume the auroral substorm (brightest auroral region) during the entire time period shown in Figure 2, maps tailward of geosynchronous orbit. The third row contains one of three events (cases 1, 3, and 6), where GOES is strongly displaced in the east-west direction from the pseudobreakup and substorm onset location. In the shown event, it takes 10–20 min until the expanding bright auroral region reaches the mapped GOES position. In the last row, one of the four events is shown where GOES appears equatorward of the pseudobreakup and of the substorm breakup (cases 4, 5, 7 and 10). However, because of a continued equatorward motion of the nightside low-latitude boundary during substorm expansion, the brightest auroral region extends to the mapped GOES position some tens of minutes after substorm onset. Not shown in Figure 2 is the event where GOES appears along the poleward oval boundary (case 9).

[30] The results from the image analysis are summarized in Tables 2 and 3. Table 2 gives information about whether GOES maps inside or outside the oval. Table 3 lists the distance between GOES and auroral breakup for all events.

4.2.1. Mapped GOES Location Relative to the Oval Boundaries

[31] In Table 2 the latitudes of the GOES mapped position in the ionosphere, and of the equatorward oval boundary at the GOES longitude are given for three different points in time: at pseudobreakup start, at substorm onset, and at the point in time where a clear dipolarization starts in GOES *B* field data. For the oval boundary determination we have used Polar UV images in the LBHL mode closest to the times of interests (for 23 times, an LBHL image exists, in 5 cases an LBHL image exists 1 min later, in 2 cases, 3 min later). The equatorward oval boundary is defined as the low-latitude limit where the auroral brightness has dropped to 1/3 of its maximum value along the longitude of the mapped GOES position. This method has been shown by *Baker et al.* [2000] to be superior to boundary definitions using a constant brightness threshold. A latitude range instead of an exact number is given in those events (cases 8 and 9) where an exact boundary determination is not possible owing to a bad Polar UV image quality at lowest latitudes, which is caused by a very flat inclination angle of the satellite to the polar ionosphere. Fortunately, this does not affect our results as GOES maps far poleward from the low-latitude oval boundary in these two events: into the breakup region and to the poleward oval boundary for case 8 and case 9, respectively. GOES latitude is highlighted in bold for those points in time where GOES maps inside the oval.

[32] Not given in Table 2 are the poleward oval boundaries, as GOES is always equatorward of this boundary, except in case 9. In that event, GOES maps at the pseudobreakup and onset to the poleward oval boundary. At the point in time where the large-scale dipolarization is registered, GOES is located within the oval due to a poleward motion of the high-latitude oval boundary during substorm expansion (at dipolarization start, GOES position maps 0.7° equatorward from the poleward oval boundary).

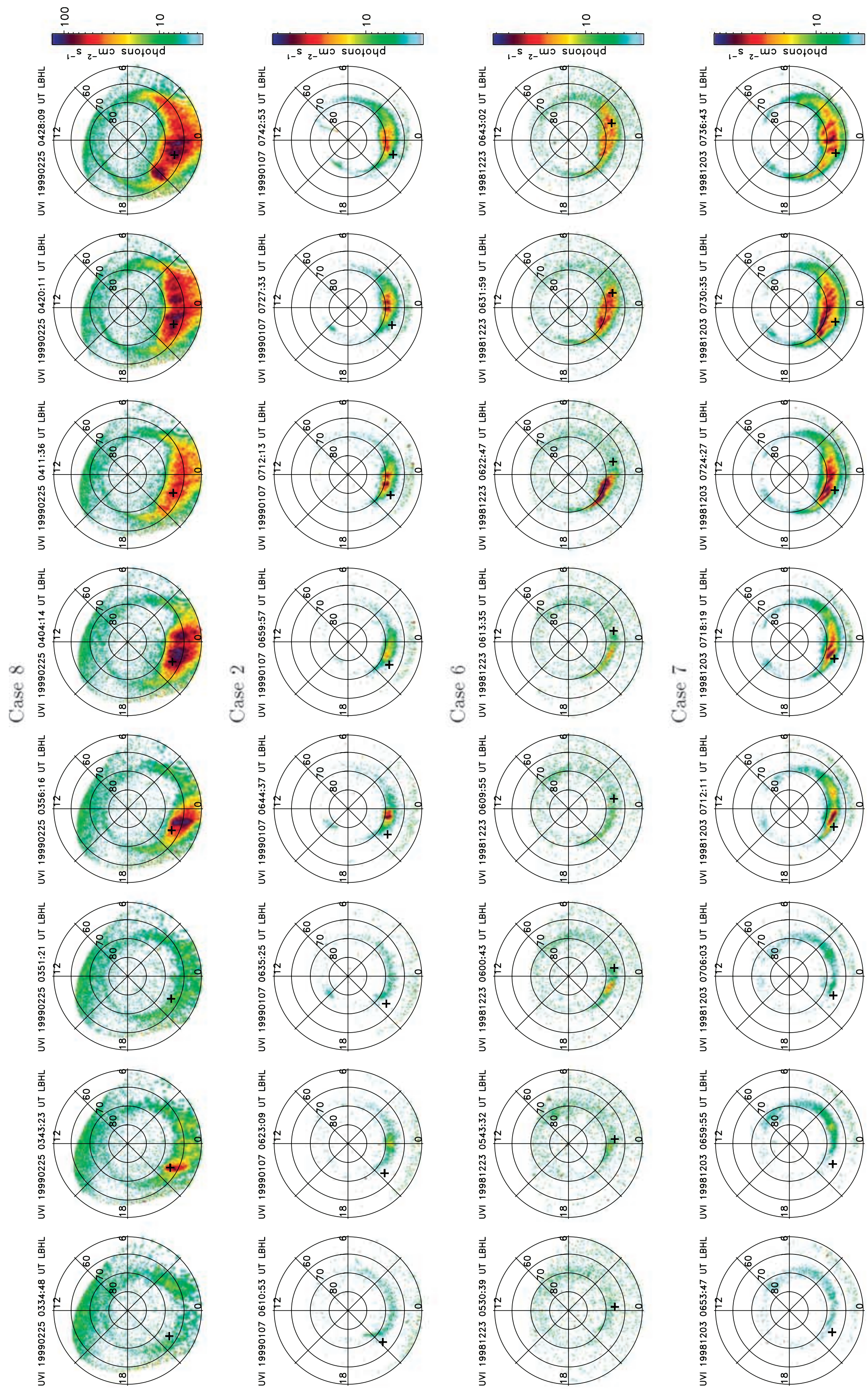

Figure 2

Table 2. Latitude of GOES and Equatorward Oval Boundary at GOES Longitude[a]

		Pseudobreakup		Substorm Onset		Dipolarization at GOES	
Case	Date	GOES Latitude	Oval Boundary	GOES Latitude	Oval Boundary	GOES Latitude	Oval Boundary
8	25 Feb 1999	**64.0**	55.5–58?	**64.0**	54–56.5?	**64.0**	55.2–56.2?
3	28 Dec 1998	65.2	66.0	**65.3**	63.5	**65.3**	63.1
1	7 Jan 1999a	64.8	64.9	**64.7**	64.6	**64.7**	64.7
6	23 Dec 1998	65.3	65.7	**65.4**	63.5	**65.4**	62.3
5	14 Dec 1998	64.5	66.1	64.4	65.4	**64.5**	64.3
7	3 Dec 1998	64.5	66.0	64.5	65.3	64.5	64.8
9	24 Feb 1999	63.6 polew. board.	55–58?	63.6 polew. board.	54–57.5?	**63.7**	56.5–57.5?
4	6 Dec 1998	65.2	67.3	65.2	66.0	**65.2**	64.2
10	15 Jan 1999	**62.7**	61.5	**62.7**	61.5	**62.7**	60.5
2	7 Jan 1999b	65.0	67.5	65.0	66.0	**-**	no dipolariz.

[a]In degrees CGLat. GOES latitude is highlighted in bold for those points in time where GOES maps inside the oval.

[33] Table 2 shows that in most cases, the low-latitude oval boundary moves equatorward not only between pseudobreakup and substorm onset but even during substorm expansion. The average low-latitude boundary location is 63.8° CGLat at pseudobreakup, 62.7° CGLat at substorm onset, and 61.8° CGLat when the dipolarization starts at GOES. The latitude of GOES foot point hardly changes during the analyzed time span. Comparing the location of GOES relative to the oval boundary, it is seen that at nearly all pseudobreakups GOES appears equatorward of the oval. Even at substorm onset, GOES is in half of the cases still equatorward of the oval boundary, while at the point in time when the large-scale dipolarization is registered at GOES, the satellite maps in nearly all events (except in case 7) inside the oval.

4.2.2. Mapped GOES Distance From the Breakup Region and Propagation Speed of the Dipolarization Region

[34] Table 3 gives the latitudinal (in degrees CGLat) and longitudinal distance (in MLT) between the mapped GOES position and substorm breakup for all events. A positive longitudinal (latitudinal) distance means an eastward (poleward) displacement of GOES from the breakup region. At the point in time where the auroral breakup becomes clearly visible in the Polar UV images, it appears as a broad spot with a diameter of 2°–5° latitude. Thus, the exact location of the original growth-phase arc cannot be determined. Here, the point of the highest intensity within the breakup region is taken as an approximation of the onset location. The events are sorted as in Table 2 after the time span between onset and dipolarization start. The delay times are given explicitly in column 2 of Table 3. Marked in bold are all cases with a large azimuthal displacement ($\geq$1.7 MLT) and all cases with a large radial displacement of GOES from the breakup region ($\geq$2.0° CGLat). For an easier comparison, the results of Table 2 are summarized in column 6. In the last column, the direction of the dipolarization propagation toward GOES and its propagation speed are given.

[35] Table 3 shows, in the event where no dipolarization is seen at all (case 2), the mapped GOES position appears during the entire event equatorward of the oval (see also Figure 2). The event with the closest onset-GOES distance (case 8) has the shortest dipolarization delay (2 min). As can be seen from Figure 2, although GOES is strongly polewardly displaced from the brightest point of the breakup location, it is still inside the (broad) breakup region. Thus, the propagation of the dipolarization region is mainly in the westward direction, with a propagation speed of 0.55 MLT min^{-1}. In the remaining events with a relatively short time delay (8–17 min), GOES maps to the oval. GOES is less than 2° latitude away from the auroral breakup, but is strongly displaced from the auroral breakup region in duskward or dawnward direction (cases 1, 3, and 6). Thus, it is highly probable that even in these cases, the dipolarization delay is mainly caused by a propagation of the dipolarization region in the azimuthal direction. The average azimuthal propagation speeds can be estimated in these three cases as 0.33 MLT min^{-1}, 0.1 MLT min^{-1}, and $-$0.24 MLT min^{-1}, respectively (positive sign means eastward propagation). Including case 8, the average velocity of the dipolarization spread in azimuthal direction is thus 0.22 MLT min^{-1}. The four events with a large equatorward displacement of GOES from the breakup region (cases 4, 5, 7 and 10) have extremely long dipolarization time delays (22–31 min). In all four events, GOES is located less than 1.1 MLT but several degrees latitude away from the auroral breakup region. Thus, the time delay is for these cases most likely connected to a strongly retarded dipolarization spread or alternatively, a stepwise or an extremely slow earthward propagation of the dipolarization region. With the present data set it is not possible to determine which is the correct scenario. Assuming a constant earthward spread of the dipolarization region, the earthward propagation speed becomes in these four cases 0.095, 0.080° min^{-1}, 0.114° min^{-1}, and 0.081° min^{-1}. The resulting average earthward propagation speed is 0.09° min^{-1}. For case 9 (where GOES

Figure 2. Polar UV images of four different growth-phase pseudobreakups and subsequent substorm breakups. The plots show a polar view on the Northern Hemisphere, with overlaid MLT-CGLat coordinates. The black crosses mark the mapped position of the GOES satellite on the polar plot (using the T96 model). From top to bottom, four different pseudobreakup events are shown: case 8, GOES in the source region of pseudobreakup and substorm breakup; case 2, GOES always equatorward (earthward) of the source region, case 6, GOES in the source region after an eastward expansion of the auroral substorm; and case 7, GOES in the source region after an equatorward expansion of the nightside oval.

Table 3. Dipolarization Time Delay, Distance Between Substorm Breakup and the Mapped GOES Position, and Estimated Speed of the Dipolarization Expansion[a]

Case	Date	Dipolarization Delay (min)	GOES Onset Distance Longitude (MLT)	GOES Onset Distance Latitude (deg)	GOES Location at Onset	Dipolarization Speed and Direction
8	25 Feb 1999	2	−1.1	**+6.3**	inside oval	0.55 MLT min^{-1} westward
3	28 Dec 1998	8	**+2.6**	−1.9	inside oval	0.33 MLT min^{-1} eastward
1	7 Jan 1999a	11	**−2.6**	−1.3	inside oval	0.24 MLT min^{-1} westward
6	23 Dec 1998	17	**+1.7**	−1.4	inside oval	0.1 MLT min^{-1} eastward
5	14 Dec 1998	22	+0.1	**−2.1**	outside oval	0.10° min^{-1} equatorward
7	3 Dec 1998	25	−0.8	**−2.0**	outside oval	0.08° min^{-1} equatorward
9	24 Feb 1999	26	+1.4	**+3.1**	at polew. bound.	poleward and eastward
4	6 Dec 1998	29	−0.2	**−3.3**	outside oval	0.11° min^{-1} equatorward
10	15 Jan 1999	31	+1.1	**−2.5**	inside oval	0.08° min^{-1} equatorward
2	7 Jan 1999b	-	**−1.8**	**−2.0**	outside oval	no dipolarization

[a]Marked in bold are all cases with a large azimuthal displacement (≥1.7 MLT) and all cases with a large radial displacement of the mapped GOES position from the breakup region (≥2.0° CGLat).

at substorm onset maps to the poleward oval boundary) it is not possible to estimate the propagation speed of the dipolarization region. The poleward motion of the high-latitude oval boundary and the dawnward expansion of the bright auroral region take place in a rather irregular way. Also, a large part of the oval appears not very clearly in the Polar UV images owing to a too low inclination angle.

4.3. Auroral Bulge Expansion and Expansion of Tail Dipolarization Region

[36] The dependence of the dipolarization delay on the distance between the mapped GOES position and auroral breakup location indicates a possible connection between the expansion of the auroral bulge and the expansion of the tail dipolarization region. Comparing GOES *B* field data with the substorm evolution, as it appears on the UV images, reveals that the start of a strong dipolarization appears approximately when the expanding bright auroral region has reached the mapped GOES position. In the events with a long dipolarization time delay, an equatorward expansion of the bright auroral region parallel to the equatorward oval expansion is responsible for an overlap with the GOES location. For the events with a short time delay, the region of dynamic auroral displays reaches the GOES owing to a dawn-duskward expansion of the auroral bulge. However, the exact timing of the local dipolarization onset at GOES cannot be predicted from the UV images. The strong brightness variations between substorms of different strengths makes a correct comparison of the auroral substorm expansions difficult. Depending on the chosen color scale for the images, the auroral bulge seems to reach the mapped GOES position up to 10 min before or after GOES registers the actual start of a strong dipolarization.

5. Discussion

5.1. Substorm Onset Determination

[37] The comparison between substorm onset (defined here as the start of the auroral breakup as identified by Polar UVI) with signatures in *AE* index, *PC* indices and *B* field variations at geosynchronous orbit in Figure 1 and Table 1 shows, substorm onset identification from these parameters would give erroneous results for our data set: *AE* increase and magnetic *B* field dipolarization at geosynchronous orbit start with a considerable time delay after onset. The correlation with the *PC* index is even worse. In those cases where a correlation with the substorm is found, the time span between *PC* increase and onset varies widely. These results are in agreement with *Liou et al.* [1999], who has shown that the best onset identification is the visual determination of the auroral breakup, as most substorm onset identifiers are subject to propagation-related delays.

[38] As seen from Figure 1, very weak substorms leave hardly any signatures at all in geosynchronous *B* field data, *AE*, and *PC* indices. This is the reason why most studies focus on strong substorms, where parameter changes above a certain level are used as a precondition for the event selection [e.g., *Liou et al.*, 2002; *Hsu and McPherron*, 2003]. Because of the identification of pseudobreakups exclusively from auroral images, the present data set covers even those pseudobreakups occurring before small substorms on a strongly contracted oval. Small substorms have been shown by *Kullen and Karlsson* [2004] to be the substorm type that is most commonly preceded by pseudobreakups.

5.2. *PC* Indices: Relation to Substorm Evolution and Interhemispheric Differences

[39] From Figure 1 and Table 1 we find that the unified *PC* indices do not correlate well with the solar wind merging field E_m. As mentioned above, this is probably connected to the only weakly southward or northward IMF conditions during most substorms of our data set [*Troshichev et al.*, 2006]. The similarity of *PC* and *AE* index curves in the stronger substorm events shows that in these cases, the *PC* indices are mainly influenced by the evolution of the auroral substorm. This result is not surprising. *Janzhura et al.* [2007] showed that independent on solar wind conditions and season, the correlation with the *AE* index (r = 0.7–0.85) is significantly higher than the correlation with the solar wind merging *E* field (r = 0.63–0.66). The higher similarity between winter (northern) *PC* index (as compared to the summer *PC* index) and *AE* index curve in our data set is expected as well from *Janzhura et al.*'s [2007] results.

[40] Surprisingly, in the strongest substorm cases, a clear bump can be discerned in the *PC* index curves while the

pseudobreakup takes place. Further investigations would be necessary to find out whether the slightly better correspondence between pseudobreakup and southern *PC* index in 3 of 4 cases is a coincidence or has to do with a possible interhemispheric difference in substorm evolution. As differences in the calculation procedures have been removed in the new, unified *PC* indices [*Troshichev et al.*, 2006], interhemispheric deviations should be caused by real differences in magnetic field variations inside the northern and southern polar caps. The well-documented seasonal dependence of substorm evolution indicates that substorms are not conjugate. Still, it remains unclear how a clearer signature in the summer *PC* index during a pseudobreakup fits to the observed suppression of discrete arcs in the high-conductive summer hemisphere [*Newell et al.*, 1996; *Liou et al.*, 2001], and the generally weaker intensity and shorter duration of summer substorms [*Chua et al.*, 2004, and references therein].

5.3. Magnetic Field Variations at Geosynchronous Orbit

[41] In only one event (case 8), GOES is located directly at the source region of pseudobreakup and very close to substorm breakup. This allows the determination of the *B* field changes between pseudobreakup and substorm onset in the originally localized tail current disruption region. The results are in agreement with previous observations: The pseudobreakup is connected to a short-duration *B* field change from taillike to dipole-like [e.g., *Ohtani et al.*, 1993; *Nakamura et al.*, 1994; *Aikio et al.*, 1999]. Between pseudobreakup and substorm breakup the *B* field stretching continues until 2 min after onset when a strong dipolarization starts. That substorm growth phase continues after the pseudobreakup with further *B* field stretching, tail current thinning and intensification, seems to be a common signature of growth-phase pseudobreakups [e.g., *Nakamura et al.*, 1994; *Ohtani et al.*, 2002].

5.4. Equtorward Motion of the Low-Latitude Oval Boundary

[42] For most events an equatorward motion of the low-latitude oval boundary between pseudobreakup and substorm onset is observed (see Table 2). This is in agreement with the statistical results by *Kullen and Karlsson* [2004], who found that an equatorward expansion of the low-latitude oval boundary between pseudobreakup and substorm onset is a common phenomenon. The equatorward expansion of the low-latitude oval boundary appears not only between pseudobreakup and substorm onset but also after the onset. Even this is a typical feature of substorms preceded by pseudobreakups. As observed by *Kullen and Karlsson* [2004], such "expanding oval substorms" appear rarely, but in case of their occurrence they are often accompanied by growth-phase pseudobreakups.

5.5. Earthward Motion of the Inner Plasma Sheet Boundary

[43] The equatorward oval boundary can be taken as a proxy for the location of the inner (earthward) plasma sheet boundary, as the most equatorward auroral emissions coincide with the b2e boundary of DMSP data [*Kauristie et al.*,1999], which has been associated by many authors with the earthward plasma sheet boundary [e.g., *Galperin and Feldstein*, 1991]. The equatorward motion of the low-latitude oval boundary between pseudobreakup and substorm onset (see Table 2) can be assumed to correspond roughly to the earthward motion of the inner plasma sheet boundary. Possible effects of mapping differences due to a continued *B* field line stretching after pseudobreakup can be neglected. From the work of *Pulkkinen et al.* [1995] it can be estimated that the ionospheric foot point of a field line crossing the equatorial plane at 10 R_E differs about one degree between a quiet time and a completely stretched magnetosphere. As most substorms appear within minutes after the pseudobreakup decayed, the continued *B* field stretching within that time span must be only a fraction of 1° latitude, which is significantly smaller than the observed 1–2 degrees oval boundary motions in Table 2. Also, the equatorward oval boundary maps far inward of 10 Re, where the strong geomagnetic field dominates over mapping effects. The earthward motion of the inner plasma sheet boundary that is typically observed during substorm growth phase, is explained by *Lyons et al.* [1999] as a continued increase of plasma convection during continued solar wind driving during geomagnetic active times.

[44] The mapped GOES distance to the equatorward oval boundary indicates the satellite location relative to the inner plasma sheet boundary: Table 2 shows that during all pseudobreakups, GOES is situated earthward of the inner plasma sheet boundary. Because of the motion of that boundary, GOES (orbiting at a fixed geocentric distance) appears at some point between the pseudobreakup and the dipolarization inside the plasma sheet. This may be part of the reason for the long dipolarization delays registered in GOES *B* field data. Probably regions earthward of the plasma sheet that are dominated by the strong geomagnetic field, do not register much from dipolarization events further downtail.

5.6. Propagation Speed of the Tail Dipolarization Region

[45] A further *B* field line stretching appears even after substorm onset in regions spatially separated from the breakup source region. This has been reported before by several authors [e.g., *Nagai*, 1982; *Gelpi et al.*, 1987]. As *Ohtani et al.* [1991] showed, the original substorm onset is confined to a small region in the tail, with an approximate size of 1 R_E. It spreads from there in all directions, so that away from the original tail current disruption region, the *B* field dipolarization is subject to a propagation delay.

[46] Comparing the propagation speed of the dipolarization region in Table 3 with typical numbers in other substorm studies shows that the average velocity of the dipolarization spread in azimuthal direction (0.22 MLT min^{-1}) is of the same order of magnitude as in previous reports. Even the difference between westward and eastward propagation speeds have been reported before. The numbers of *Liou et al.* [2002] (0.41 MLT min^{-1} westward, 0.33 MLT min^{-1} eastward speed) are comparable to those of the present study (0.40 MLT min^{-1} westward, and 0.22 MLT min^{-1} eastward speed). *Liou et al.* [2002] also discovered that the dipolarization region expands faster

close to the onset region than at larger distances in azimuthal direction. Also this is in agreement with our results. Other authors found similar numbers: *Nagai* [1982], e.g., reported westward and eastward propagation velocities of 0.43 MLT min^{-1} and 0.16 MLT min^{-1}, respectively. An ongoing study by J.-H. Shue et al. (personal communication, 2008) finds a dipolarization spread of 0.13 MLT min^{-1} in westward and 0.08 MLT min^{-1} in eastward direction.

[47] The propagation speed of the equatorward dipolarization spread is in average 0.09° min^{-1} for our data set, which is a factor 10 slower than the equatorward speed found by *Liou et al.* [2002] of 0.84° min^{-1}. From *Pulkkinen et al.*'s [1995] modeling work, it can be assumed that one degree latitude corresponds to 3 R_E in the near-Earth equatorial plane during a stretched magnetic field configuration. Thus, an equatorward auroral expansion of 0.09° min^{-1} corresponds to an earthward expansion velocity of the tail dipolarization region of 28 km s^{-1}. Also that number is nearly 10 times slower than the reported earthward propagation speeds of 180–240 km s^{-1} [*Russell and McPherron*, 1973; *Ohtani*, 1998]. Note that even when assuming a very strong effect of B field line stretching (which has so far been ignored) on the mapping of GOES position to the ionosphere, the average earthward speed is very low (0.13° min^{-1} for a one degree further equatorward ionospheric foot point of GOES). For a more complete comparison with previously reported dipolarization delays we refer to *Liou et al.*'s [2002] very detailed discussion of that subject. To summarize, the main difference between substorms preceded by growth-phase pseudobreakups, and substorms without those is an extremely slow, or strongly retarded earthward expansion of the dipolarization region in the former case.

5.7. Possible Conclusions for Pseudobreakup Models

[48] A comparison of Polar UV images with the mapped GOES position and GOES B field data has shown a close connection between auroral bulge expansion after onset and the expansion of the tail dipolarization region. Such a connection has been suggested by *Ohtani et al.* [1993] and has been shown by *Liou et al.* [2002] to exist for strong substorms. We thus suggest that the limited east-west expansion of the auroral bulge during the weakest substorms in our data set probably corresponds to a limitation of the azimuthal spread of the tail dipolarization region (not shown here is that in some of these cases a second GOES satellite is even further azimuthally displaced, showing nearly no dipolarization signatures). It seems that for these small substorms, at no point in time the entire tail is affected by the tail dipolarization and connected tail current disruption. These observations are an additional support for the idea put forward by many authors [e.g., *Sergeev et al.*, 1996] that there is a smooth transition between pseudobreakups (with only a localized source region) and substorms of increasing strength (the tail dipolarization of the smallest substorms extending only over a fraction of the tail width).

[49] The earthward motion of the inner plasma sheet boundary which in most cases continues between pseudobreakup and substorm onset, and the continued B field stretching outside the dipolarization region (leading to an additional thinning and intensification of the tail current sheet), possibly supplies a slightly better precondition for the next auroral activation to expand more than the pseudobreakup. On the basis of these observations, we suggest that growth-phase pseudobreakups appear when the magnetosphere has nearly reached conditions necessary for a local activation to develop into a real substorm. However, a common limit in any of the studied parameters, above which an auroral breakup develops in all cases into a full-scale substorm, has not been found. Apparently, the critical level for a global substorm expansion depends on additional parameters. Probably, also the time history of the solar wind plays a role, as it is known that the magnetosphere has a memory of about 100 min [*Bargatze et al.*, 1985].

[50] In most of the studied events, substorm expansion starts rather slowly, as indicated by low AE values up to 15 min after onset, a slow earthward motion of the inner plasma sheet boundary, and (maybe connected to that) a slow, or retarded earthward expansion of the dipolarization region. Assuming the equatorward plasma sheet motion is caused by an increased plasma convection, it means that the energy input into the magnetosphere continues to increase even after onset. Even most of the stronger substorms in our data set develop rather slowly at the beginning of the expansion phase. Possibly, magnetosphere regions next to the dipolarization region have not yet reached a state necessary for a current disruption to take place. Thus, the current disruption region cannot expand immediately. Only after a while conditions in the tail have become such that a full-scale substorm expansion can take place. Note, a delayed AE increase, and an equatorward oval boundary motion after onset has been observed also during substorms that are not preceded by pseudobreakups [e.g., *Liou et al.*, 2002]. However, in the latter case, the development between onset and a full-scale substorm takes a few minutes only, probably because of the much higher energy transfer into the magnetosphere, or otherwise favorable conditions in the magnetosphere created, e.g., during preceding substorms.

6. Summary

[51] This is the first comprehensive study that compares the global auroral evolution of growth-phase pseudobreakups and subsequent substorms with magnetic field variations in several different space regions. The study contains 10 events during winter 1998–1999 that have been identified exclusively from visual inspection of global auroral UV images of the northern hemisphere using the Polar spacecraft. To gain more knowledge about how ionosphere, near-Earth tail and solar wind are coupled during such events, the auroral evolution during pseudobreakup, onset and substorm expansion is compared to magnetic field variations at geosynchronous orbit (using GOES satellite data), along the auroral zone (AE index), above the polar caps (unified northern and southern PC indices) and in the solar wind (IMF B_Z and merging electric field). A detailed investigation of these parameters has confirmed a number of previous results, and resulted in several interesting new observations.

[52] 1. The IMF is predominantly southward 1–2 h around the pseudobreakup event. During or up to 10 min before the pseudobreakup IMF B_Z has temporarily near zero values.

[53] 2. Substorm onset is in this study defined as the start of the auroral substorm breakup as determined by UV images. A comparison between *AE* index and onset reveals a clear connection between onset and an increase in the *AE* index, except for the two weakest substorms where no *AE* variations are seen. In the other cases, the sharp rise in the *AE* curve appears with a time delay of 5–15 min. Pseudobreakups leave (nearly) no signatures in the *AE* index.

[54] 3. In the present data set, no clear correlation between solar wind merging *E* field and *PC* index is found, probably because of northward or small southward IMF conditions during most pseudobreakups and substorms. A clear connection between *PC* indices and substorm evolution is found only for the stronger substorm events. As expected, the winter (northern) *PC* index correlates better with the *AE* index than the summer (southern) *PC* index. As shown in previous studies, the *PC* indices rises before the *AE* index. However, the time span between *PC* index increase and substorm onset varies strongly from case to case. In the four strongest substorm cases, a bump appears in connection with the pseudobreakup that is more clearly pronounced in the southern than in the northern *PC* index.

[55] 4. It is known that the tail current disruption and connected tail dipolarization start locally at substorm onset and expand from there in all directions. In this work, it is shown that for substorms preceded by growth-phase pseudobreakups, the average azimuthal propagation speed has the same order of magnitude as reported in previous studies, whereas the average earthward propagation speed is an order of magnitude smaller than during typical substorms.

[56] 5. In nearly all cases, the equatorward UV oval boundary moves to lower latitudes between pseudobreakup and substorm onset. For most events this motion continues even during a large part of the substorm expansion phase. Assuming, this motion is connected to an earthward motion of the inner plasma sheet boundary, it can be expected that an increased earthward plasma convection continues even after substorm onset.

[57] 6. A comparison between the evolution of the auroral substorm and the time delay of the tail dipolarization after onset reveals a close connection between the expansion of the auroral substorm and the expansion of the tail dipolarization region. Thus, the small azimuthal expansion of the two smallest auroral substorms of our data set indicates an only limited azimuthal expansion of the tail dipolarization region in these cases. This implies that there is a smooth transition between pseudobreakups (having a very localized tail source region) and substorms of increasing size (the tail source region extending over the entire tail only in the stronger substorm cases).

[58] **Acknowledgments.** We are grateful to P. Stauning for helpful discussions and for providing the unified *PC* index data. We thank the CDA Web and the GOES team for providing GOES data. We acknowledge G. Parks as the principal investigator for the Polar UV imager as well as the ACE, IMP 8, and Wind instrument teams for providing magnetometer and plasma data through the GSFC/SPDF OMNIWeb interface at http://omniweb.gsfc.nasa.gov. We thank the WDC-C2 Kyoto *AE* index service, the *AE* stations, and the persons who derive the index for access to *AE* index data on the Internet.

[59] Wolfgang Baumjohann thanks Oleg Troshichev and another reviewer for their assistance in evaluating this paper.

References

Aikio, A. T., V. A. Sergeev, M. A. Shukhtina, L. I. Vagina, V. Angelopoulos, and G. D. Reeves (1999), Characteristics of pseudobreakups and substorms observed in the ionosphere, at geosynchronous orbit, and in the midtail, *J. Geophys. Res.*, *104*, 12,263, doi:10.1029/1999JA900118.

Akasofu, S.-I. (1964), The development of the auroral substorm, *Planet. Space Sci.*, *12*, 273, doi:10.1016/0032-0633(64)90151-5.

Akasofu, S.-I. (1980), The solar wind-magnetosphere energy coupling and magnetospheric disturbances, *Planet. Space Sci.*, *28*, 495, doi:10.1016/0032-0633(80)90031-8.

Baker, J., C. Clauer, A. Ridley, V. Papitashvili, M. Brittnacher, and P. Newell (2000), The nightside poleward boundary of the auroral oval as seen by DMSP and the Ultraviolet Imager, *J. Geophys. Res.*, *105*, 21,267, doi:10.1029/1999JA000363.

Baker, D. N., et al. (2002), Timing of magnetic reconnection initiation during a global magnetospheric substorm onset, *Geophys. Res. Lett.*, *29*(24), 2190, doi:10.1029/2002GL015539.

Bargatze, L. F., D. N. Baker, R. L. McPherron, and E. W. Hones (1985), Magnetospheric impulse response for many levels of geomagnetic activity, *J. Geophys. Res.*, *90*, 6387, doi:10.1029/JA090iA07p06387.

Chua, D., G. Parks, M. Brittnacher, G. Germany, and J. Spann (2004), Auroral substorm timescales: IMF and seasonal variations, *J. Geophys. Res.*, *109*, A03207, doi:10.1029/2003JA009951.

Cummings, W. D., J. N. Barfield, and P. J. Coleman (1968), Magnetospheric substorms observed at synchronous orbit, *J. Geophys. Res.*, *73*, 6687, doi:10.1029/JA073i021p06687.

Elvey, C. T. (1957), Problems of auroral morphology, *Proc. Natl. Acad. Sci. U. S. A.*, *43*, 63.

Galperin, Y. I., and Y. I. Feldstein (1991), Auroral luminosity and its relationship to magnetospheric plasma domains, in *Auroral Physics*, edited by C.-I. Meng, M. J. Rycroft, and L. A. Frank, p. 207, Cambridge Univ. Press, New York.

Gelpi, C., H. J. Singer, and W. J. Hughes (1987), A comparison of magnetic signatures and DMSP auroral images at substorm onset: Three case studies, *J. Geophys. Res.*, *92*, 2447, doi:10.1029/JA092iA03p02447.

Gerard, J.-C., B. Hubert, A. Gerard, and M. Meurant (2004), Solar wind control of auroral substorm onset locations observed with the IMAGE-FUV imagers, *J. Geophys. Res.*, *109*, A03208, doi:10.1029/2003JA010129.

Germany, G. A., J. F. Spann, G. K. Parks, M. J. Brittnacher, R. Elsen, L. Chen, D. Lummerzheim, and M. H. Rees (1998), Auroral observations from the POLAR Ultraviolet Imager (UVI), in *Geospace Mass and Energy Flow: Results From the International Solar-Terrestrial Physics Program*, *Geophys., Monogr. Ser.*, vol. 104, edited by J. L. Horwitz, D. L. Gallagh, and W. K. Peterson, p. 149, AGU, Washington, D. C.

Henderson, M. G., G. D. Reeves, and J. S. Murphy (1998), Are north-south structures an ionospheric manifestation of bursty bulk flows?, *Geophys. Res. Lett.*, *25*, 3737, doi:10.1029/98GL02692.

Hsu, T.-S., and R. L. McPherron (2003), Occurrence frequencies of IMF triggered and nontriggered substorms, *J. Geophys. Res.*, *108*(A7), 1307, doi:10.1029/2002JA009442.

Jacquey, C., J.-A. Sauvaud, and J. Dandouras (1991), Location and propagation of the magnetotail current disruption during substorm expansion: Analysis and simulation of an ISEE multi-onset event, *Geophys. Res. Lett.*, *18*, 389, doi:10.1029/90GL02789.

Janzhura, A., O. Troshichev, and P. Stauning (2007), Unified *PC* indices: Relation to isolated magnetic substorms, *J. Geophys. Res.*, *112*, A09207, doi:10.1029/2006JA012132.

Kan, J. R., and L. C. Lee (1979), Energy coupling function and solar wind magnetosphere dynamo, *Geophys. Res. Lett.*, *6*, 577, doi:10.1029/GL006i007p00577.

Kauristie, K., J. Weygand, T. I. Pulkkinen, J. S. Murphree, and P. T. Newell (1999), Size of the auroral oval: UV ovals and precipitation boundaries compared, *J. Geophys. Res.*, *104*, 2321, doi:10.1029/1998JA900046.

Kennel, C. (1992), The Kiruna conjecture: The strong version, in *Proceedings of ICS-1*, *Eur. Space Agency Spec. Publ.*, *ESA SP-335*, 599.

King, J. H., and N. E. Papitashvili (2005), Solar wind spatial scales in and comparisons of hourly Wind and ACE plasma and magnetic field data, *J. Geophys. Res.*, *110*, A02104, doi:10.1029/2004JA010649.

Kokubun, S., and R. L. McPherron (1981), Substorm signatures at synchronous altitude, *J. Geophys. Res.*, *86*, 11,265, doi:10.1029/JA086iA13p11265.

Koskinen, H. E. J, R. E. Lopez, R. J. Pellinen, T. I. Pulkkinen, D. N. Baker, and T. Bosinger (1993), Pseudobreakup and substorm growth-phase in the ionosphere and magnetosphere, *J. Geophys. Res.*, *98*, 5801, doi:10.1029/92JA02482.

Kullen, A., and T. Karlsson (2004), On the relation between solar wind, pseudobreakups, and substorms, *J. Geophys. Res.*, *109*, A12218, doi:10.1029/2004JA010488.

Liou, K., C.-I. Meng, A. T. Y. Lui, P. T. Newell, M. Brittnacher, G. Parks, G. D. Reeves, R. R. Anderson, and K. Yumoto (1999), On relative timing in substorm onset signatures, *J. Geophys. Res.*, *104*, 22,807, doi:10.1029/1999JA900206.

Liou, K., P. T. Newell, and C.-I. Meng (2001), Seasonal effects on auroral particle acceleration and precipitation, *J. Geophys. Res.*, *106*, 5531, doi:10.1029/1999JA000391.

Liou, K., C.-I. Meng, A. T. Y. Lui, P. T. Newell, and S. Wing (2002), Magnetic dipolarization with substorm expansion onset, *J. Geophys. Res.*, *107*(A7), 1131, doi:10.1029/2001JA000179.

Lui, A. T. Y. (1991), A synthesis of magnetospheric substorm models, *J. Geophys. Res.*, *96*, 1849, doi:10.1029/90JA02430.

Lui, A. T. Y. (1996), Current disruption in the Earth's magnetosphere: Observations and models, *J. Geophys. Res.*, *101*, 13,067, doi:10.1029/96JA00079.

Lui, A. T. Y., S.-I. Akasofu, E. W. Hones Jr., S. J. Bame, and C. E. McIlwain (1976), Observations of the plasma sheet during a contracted oval substorm in a prolonged quiet period, *J. Geophys. Res.*, *81*, 1415, doi:10.1029/JA081i007p01415.

Lukianova, R., O. Troshichev, and G. Lu (2002), The polar cap magnetic activity indices in the southern (PCS) and northern (PCN) polar caps: Consistency and discrepancy, *Geophys. Res. Lett.*, *29*(18), 1879, doi:10.1029/2002GL015179.

Lyons, L. R., T. Nagai, G. T. Blanchard, J. C. Samson, T. Yamamoto, T. Mukai, A. Nishida, and S. Kokubun (1999), Association between Geotail plasma flows and auroral poleward boundary intensifications observed by CANOPUS photometers, *J. Geophys. Res.*, *104*, 4485, doi:10.1029/1998JA900140.

McPherron, R. L. (1972), Substorm related changes in the geomagnetic tail: The growth phase, *Planet. Space Sci.*, *20*, 1521, doi:10.1016/0032-0633(72)90054-2.

Nagai, T. (1982), Observed magnetic substorm signatures at synchronous altitude, *J. Geophys. Res.*, *87*, 4405, doi:10.1029/JA087iA06p04405.

Nakamura, M., D. N. Baker, T. Yamamoto, R. D. Belian, E. A. Bering III, J. R. Benbrook, and J. R. Theall (1994), Particle and field signatures during pseudobreakup and major expansion onset, *J. Geophys. Res.*, *99*, 207, doi:10.1029/93JA02207.

Newell, P. T., C.-I. Meng, and K. M. Lyons (1996), Suppression of discrete aurorae by sunlight, *Nature*, *381*, 766, doi:10.1038/381766a0.

Ohtani, S. (1998), Earthward expansion of tail current disruption: Dual-satellite study, *J. Geophys. Res.*, *103*, 6815, doi:10.1029/98JA00013.

Ohtani, S., K. Takahashi, L. J. Zanetti, T. A. Potemra, R. W. McEntire, and T. Iijima (1991), Tail current disruption in the geosynchronous region, in *Magnetospheric Substorms*, *Geophys. Monogr. Ser.*, vol. 64, p. 131, AGU, Washington, D. C.

Ohtani, S., S. Kokubun, and C. T. Russell (1992), Radial expansion of the tail current disruption during substorms: A new approach to the substorm onset region, *J. Geophys. Res.*, *97*, 3129, doi:10.1029/91JA02470.

Ohtani, S., et al. (1993), A multisatellite study of a pseudo-substorm onset in the near-Earth magnetotail, *J. Geophys. Res.*, *98*, 19,355, doi:10.1029/93JA01421.

Ohtani, S., R. Yamaguchi, H. Kawano, F. Creutzberg, J. B. Sigwarth, L. A. Frank, and T. Mukai (2002), Does the braking of the fast plasma flow trigger a substorm?: A study of the August 14, 1996, event, *Geophys. Res. Lett.*, *29*(15), 1721, doi:10.1029/2001GL013785.

Ohtani, S., H. J. Singer, and T. Mukai (2006), Effects of the fast plasma sheet flow on the geosynchronous magnetic configuration: Geotail and GOES coordinated study, *J. Geophys. Res.*, *111*, A01204, doi:10.1029/2005JA011383.

Partamies, N., O. Amm, K. Kauristie, T. I. Pulkkinen, and E. Tanskanen (2003), A pseudo-breakup observation: Localized current wedge across the postmidnight auroral oval, *J. Geophys. Res.*, *108*(A1), 1020, doi:10.1029/2002JA009276.

Pulkkinen, T. I., D. N. Baker, R. J. Pellinen, J. S. Murphree, and L. A. Frank (1995), Mapping of the auroral oval and individual arcs during substorms, *J. Geophys. Res.*, *100*, 21,987.

Pulkkinen, T. I., D. N. Baker, M. Wiltberger, C. Goodrich, R. E. Lopez, and J. G. Lyon (1998), Pseudobreakup and substorm onset: Observations and MHD simulations compared, *J. Geophys. Res.*, *103*, 14,847, doi:10.1029/97JA03244.

Rostoker, G. (1998), On the place of the pseudo-breakup in a magnetospheric substorm, *Geophys. Res. Lett.*, *25*, 217, doi:10.1029/97GL03583.

Rostoker, G. (2002), Identification of substorm expansive phase onsets, *J. Geophys. Res.*, *107*(A7), 1137, doi:10.1029/2001JA003504.

Rostoker, G., S.-I. Akasofu, J. Foster, R. A. Greenwald, Y. Kamide, K. Kawasaki, A. T. Y. Lui, R. L. McPherron, and C. T. Russell (1980), Magnetospheric substorms—Definition and signatures, *J. Geophys. Res.*, *85*, 1663, doi:10.1029/JA085iA04p01663.

Russell, C. T., and R. L. McPherron (1973), The magnetotail and substorms, *Space Sci. Rev.*, *15*, 205, doi:10.1007/BF00169321.

Sergeev, V. A., T. I. Pulkkinen, and R. J. Pellinen (1996), Coupled-mode scenario for the magnetospheric dynamics, *J. Geophys. Res.*, *101*, 13,047, doi:10.1029/95JA03192.

Torr, M. R., et al. (1995), A far ultraviolet imager for the international solar-terrestrial physics mission, *Space Sci. Rev.*, *71*, 329, doi:10.1007/BF00751335.

Troshichev, O. A., and R. Y. Lukianova (2002), Relation of PC index to the solar wind parameters and substorm activity in time of magnetic storms, *J. Atmos. Sol. Terr. Phys.*, *64*, 585.

Troshichev, O. A., N. P. Dmitrieva, and B. M. Kuznetsov (1979), Polar cap magnetic activity as a signature of substorm development, *Planet. Space Sci.*, *27*, 217, doi:10.1016/0032-0633(79)90063-1.

Troshichev, O. A., V. G. Andrezen, S. Vennerstrom, and E. Friis-Christensen (1988), Magnetic activity in the polar cap—A new index, *Planet. Space Sci.*, *36*, 1095, doi:10.1016/0032-0633(88)90063-3.

Troshichev, O., A. Janzhura, and P. Stauning (2006), Unified PCN and PCS indices: Method of calculation, physical sense, and dependence on the IMF azimuthal and northward components, *J. Geophys. Res.*, *111*, A05208, doi:10.1029/2005JA011402.

Tsyganenko, N. A. (1989), A magnetospheric magnetic field model with a warped tail current sheet, *Planet. Space Sci.*, *37*, 5, doi:10.1016/0032-0633(89)90066-4.

Tsyganenko, N. A. (1995), Modeling the Earth's magnetospheric magnetic field confined within a realistic magnetopause, *J. Geophys. Res.*, *100*, 5599, doi:10.1029/94JA03193.

Zhou, X., and B. T. Tsurutani (1999), Rapid intensification and propagation of the dayside aurora: Large scale interplanetary pressure pulses (fast shocks), *Geophys. Res. Lett.*, *26*, 1097, doi:10.1029/1999GL900173.

T. Karlsson, Division of Space and Plasma Physics, School of Electrical Engineering, KTH, SE-10044 Stockholm, Sweden. (tomas.karlsson@ee.kth.se)

A. Kullen, Swedish Institute of Space Physics, Box 537, SE-75121 Uppsala, Sweden. (kullen@irfu.se)

S. Ohtani, Johns Hopkins University Applied Physics Laboratory, 11100 Johns Hopkins Road, Laurel, MD 20723, USA. (shin.ohtani@jhuapl.edu)